Science
AAAS

Supplementary Materials for

The G protein signaling regulator RGS3 enhances the GTPase activity of KRAS

Chuanchuan Li *et al.*

Corresponding author: Piro Lito, litop@mskcc.org

Science **374**, 197 (2021)
DOI: 10.1126/science.abf1730

The PDF file includes:

Other Supplementary Material for this manuscript includes the following:

Materials and Methods

Cell culture and reagents

All cell lines used in this study were maintained in DMEM medium supplemented with 10% FBS, penicillin, streptomycin and 2 mM L-glutamine. Cell lines were obtained from ATCC (H358: CRL-5807; H2122: CRL-5985; H2030: CRL-5914; SW1573: CRL-2170), expanded immediately and frozen in aliquots. The cell lines tested negative for mycoplasma. All experiments were performed within 20 passages. ARS1620 and ARS853 were purchased from MedChemExpress. Antibodies targeting RGS3 (sc-100762, 1:1,000) and GST (sc-138, 1:5000) were purchased from Santa Cruz Biotechnology. Antibodies targeting KRAS (WH0003845M1, 1:1,000), FLAG (F1804, 1:1,000) were obtained from Sigma. Antibodies targeting HA (C29F4 or 3724,1:1000) or His (2365S, 1:1000) were obtained from Cell Signaling Technology. The BRAF specific antibody (sc-9002, 1:1,000) was purchased from Santa Cruz Biotechnology. The antibody dilution during immunoblotting is shown.

Plasmids

For recombinant protein expression, DNA sequences encoding RGS3 p75 (Uniprot: P49796-1), RGS3 p25 (Uniprot: P49796-2), NF1 GAP related domain (1198-1530aa, Uniprot: P21359) and KRAS 4A (Uniprot: P01116-1) or 4B (Uniprot: P01116-2) were cloned into the pET-28a vector. The labeling of RGS3 variants in our study is based on their migration on western blotting, which differs from their predicted molecular weight. In order to generate a GST-tagged KRAS, the gene was cloned into the pGEX-4T-1 vector. For mammalian expression, *RGS3* was cloned into the pCDNA-3.1-c-FLAG vector, and *KRAS* was cloned into pCDNA-3.0-HA or pDEST27 (for GST-tagged KRAS). All indicated mutants were generated by site-directed mutagenesis. All constructs were verified by DNA sequencing.

GTPase assays

GTP[γ^{32}P] hydrolysis assay. KRAS proteins (0.5 µg) were reacted with 0.04 µM GTP[γ^{32}P] (6000 Ci/mmol; PerkinElmer Life Sciences) in 100 µL loading buffer (50 mM HEPES, pH 7.5, 50 mM NaCl, 1 mM DTT, 0.1 mM EGTA, 10 mM EDTA, and 1 mg/mL BSA) for 10 min at 30°C *(5, 31)*. Loading reactions were stopped by placing on ice and adding $MgCl_2$ to a final concentration of 20 mM. The GTPase assays were performed at 30°C in 100 µL mixtures containing 20 nM of loaded KRAS and either hydrolysis buffer (25 mM HEPES pH 7.5, 50 mM NaCl, 1 mM DTT, 1 mM $MgCl_2$ and 1 mg/mL BSA) alone, or in combination with WCE or purified RGS3 (0.08 - 0.4 µg/µL). Equimolar comparisons of NF1, RASA1 and RGS3 were carried out by using the continuous hydrolysis assay (see below). Reactions were stopped at the indicated time by filtering through 0.45-µm nitrocellulose membrane filters. The filters were washed 3 times with 0.2 mL of ice-cold hydrolysis buffer, air dried, and processed by autoradiography. Reaction rates were determined by fitting an exponential curve to normalized data (% of baseline value). For the determination of protein stability, the hydrolysis reactions were stopped by boiling at 100°C for 10 min in Laemmli buffer. The samples were then subjected to SDS-PAGE followed by Coomassie Brilliant Blue (CBB) staining or immunoblotting with a His-specific antibody.

GTP[α^{32}P] hydrolysis assay. KRAS proteins were loaded with GTP[α^{32}P] (3000 Ci/mmol; PerkinElmer Life Sciences) and subjected to the hydrolysis reaction as indicated above. Upon completion of the hydrolysis reaction and immobilization of KRAS-nucleotide complexes on nitrocellulose membranes, the nucleotides were eluted by incubating with elution buffer (50 mM

HEPES pH 7.5, 50 mM NaCl, 1 mM DTT, 0.1 mM EGTA, 0.1% SDS, 10 mM EDTA, 1 mM GTP and 1 mM GDP) for 3 min at 85°C. The released nucleotides were resolved by thin layer chromatography (TLC) on PEI cellulose F paper (Merck) with 1 M LiCl and 1 M formic acid. The TLC papers were then dried and processed by autoradiography.

Continuous hydrolysis assay (two-step detection of inorganic phosphate). The EnzChek Phosphate Assay Kit (Thermo Fisher Scientific) was used to continuously measure phosphate release in vitro following the manufacturer's recommendation *(19, 32)*. In brief, 100 µM KRAS protein were loaded with 2.5 mM GTP in assay buffer (10 mM EDTA, 30 mM Tris pH 7.5 and 1 mM DTT) at room temperature for 2h. Loaded KRAS was then desalted by gel filtration in ZebaTM spin columns (Thermo Scientific). The hydrolysis reaction was performed in 384-well microplates (Costar) containing GTP-loaded KRAS (50 µM), MESG (200 µM), PNP (5 U/mL), and $MgCl_2$ (40 mM) in reaction buffer (30 mM Tris pH 7.5,1 mM DTT). GAPs were added at a concentration of 50 µM or as indicated. The reaction was monitored by reading the absorbance at 360 nm every 10 to 20 s for ~16-60 min at room temperature. Raw values were imported to Prism and normalized by the embedded min-max normalization strategy. Kinetic constants were obtained by fitting an exponential curve. In intrinsic hydrolysis reactions, where the maximum PO_4 release was less than observed in the paired GAP-assisted reaction, the maximum value during normalization was set as the maximum value from the paired GAP-assisted reaction.

GTPase assay choice. Two-step phosphate labeling reagents are inaccurate for slow reactions. The reagent is not stable over long incubation periods, which are necessary to achieve complete hydrolysis (during intrinsic reactions) and to accurately determine the half-life. Moreover, two-step detection systems are affected by the presence of inorganic phosphate in buffers (or cellular extracts) and cannot be used to isolate cellular factors that enhance the hydrolysis rate. With these in mind, in order to calculate the intrinsic hydrolysis rate constant we relied on single-turnover [^{32}P]GTP hydrolysis assays and allowed a sufficient time for the reaction to reach a steady state maximum (i.e., undetectable levels in fig. S1C). Validation studies were carried out using [^{32}P]GTP (at the α or ɣ position) and two-step phosphate labeling reagents. The latter were also used to determine the kinetics of the GAP-assisted reactions, since these are considerably faster than intrinsic hydrolysis.

RAS-binding domain (RBD) pull-down

This was performed as described previously *(33)* by using the RAS activation kit (Thermo Scientific). Briefly, 50 µg whole cell lysates were incubated with 40 µg GST-RBD and 100 µL glutathione beads for 60 min followed by three washes in NP40 wash buffer and elution of pull-down fractions with 2×SDS PAGE loading dye. The samples were then subjected to western blotting with a KRAS specific (WH0003845M1) antibody *(34)*.

Chromatographic separation and identification of $KRAS^{G12C}$-directed GAP activity.

H358 cells were chosen as a starting point during chromatography (and as the main model system for validating studies) because these are the most sensitive to G12Ci treatment. We reasoned that extracts from these cells would be most likely to yield a successful identification of a $KRAS^{G12C}$-directed GAP.

The chromatographic separation and identification process consisted of two rounds of size-exclusion chromatography (SEC, steps 1 and 2), desalting (step 3), anion exchange chromatography (AEC, step 4) and mass spectrometry (step 5). All procedures were carried out at 4 °C by using the ÄKTA system.

H358 cells growing exponentially (2 g) were collected and resuspended in 5 mL hydrolysis buffer (25 mM HEPES, pH 7.5, 50 mM NaCl, 1 mM DTT, 1 mM $MgCl_2$). The cells were broken down by sonication and centrifuged at 13,200 rpm for 1 h to obtain the supernatant. The supernatant was passed through a 0.45 μm filter (Millipore), centrifuged at 13,200 rpm for 60 min and loaded onto a HiLoad Superdex 200PG column (GE healthcare) for the first round of SEC (step 1). The fractions (1 mL) eluted from this column were collected and a portion (5 μL) was used in a GTP[γ^{32}P] hydrolysis assay as described above.

Step 1 fractions that enhanced $KRAS^{G12C}$ hydrolysis were pooled and loaded onto Superdex 200 (GE healthcare) for the second round of SEC (step 2). Again, eluted fractions (1mL) were collected, and a portion (10 μL) was subjected to the GTP[γ^{32}P] hydrolysis assay.

Step 2 fractions that enhanced $KRAS^{G12C}$ hydrolysis were pooled, and their buffer exchanged into one containing HEPES 20 mM pH 7.5, 20 mM NaCl, DTT 1 mM (step 3) using a HiTrap desalting column (GE healthcare, 5 mL). Desalted fractions were then loaded (step 4) onto a DEAE column (GE healthcare) and washed with a buffer containing HEPES 20 mM pH 7.5, NaCl 0.5M, DTT 1 mM using a 0-100% gradient over 5 column volumes (each 25 mL). Eluded step 4 fractions (1 mL) were collected. In order to determine their GTPase enhancing effect, 30% of each fraction was concentrated to 15 μL using a using 3 kDa molecular weight cut-off centrifugal filter and subjected to the $KRAS^{G12C}$ GTP[γ^{32}P] hydrolysis assay.

AEC fractions that enhanced $KRAS^{G12C}$ hydrolysis were evaluated by mass spectrometry (step 5) to identify proteins annotated as GAPs. Proteins from active AEC fractions were precipitated with equal volume of 20% TCA/acetone for 12h at 4°C. The supernatant was removed by centrifugation at 13,200 rpm for 10 min at 4°C, and the pellet was washed three times with cold acetone. The protein precipitates were air-dried and submitted for trypsin digestion and mass spectrometry identification at a fee-for-service core facility (Columbia University Medical Center). The peptides were analyzed by liquid chromatography–tandem mass spectrometry on a Q Exactive mass spectrometer (Thermo Fisher Scientific). Proteins were identified by a database search of the fragment spectra against the UniProt protein database. We only evaluated proteins previously annotated as GAPs and that were identified in all fractions/peaks with GTPase-enhancing activity.

<u>$KRAS^{G12C}$-RGS3 interaction</u>

WCE (2 mg) from treated or untreated $KRAS^{G12C}$ mutant cells were subjected to IP with either a KRAS (sc-30) or an IgG antibody agarose-conjugate followed by immunoblotting with KRAS- or RGS3-specific monoclonal antibodies. A BRAF-specific antibody was used as a control.

To determine the presence of a direct interaction we used purified GST-tagged RGS3 GAP domain (RGSD) and His-tagged $KRAS^{G12C}$. The latter was loaded with GTPγS (a non-hydrolyzable GTP analogue) or GDP. The proteins (0.2 μM KRAS and 1.2 μM RGSD) were mixed in binding buffer

(25 mM Tris-HCl pH=7.5, 150 mM NaCl, 1% NP40, 5% glycerol and 5 mM $MgCl_2$) and incubated at 4°C for 1h. The reaction was then subject to a GST-pulldown.

GST pull-down assays

HEK293H cells (2.5×10^3) were seeded in 60 mm cell culture dishes and ~16h later the cells were transfected with 2 μg of GST-tagged constructs and 2 μg of FLAG-tagged constructs by using Lipofectamine 2000 (Thermo Scientific) at a ratio of 1 μg to 2 μL. 24h post-transfection, the cells were washed with 3 mL ice-cold PBS, collected and immediately centrifuged at 2000 rpm for 3 min. The cell pellets were lysed in 300 μL of NP40 lysis buffer (50 mM Tris-HCl pH=7.5, 150 mM NaCl, 1% NP40, 10% glycerol and 1 mM EDTA) supplemented with protease and phosphatase inhibitors and mixed vigorously. After incubating on ice for 10 min, the samples were centrifuged at 13,200 rpm at 4°C for 10 min. The supernatants (1 mg) were incubated and rotated with 100 μL of glutathione-sepharose beads for 60 min at 4°C and washed three times with wash buffer (25 mM Tris-HCl pH=7.5, 150 mM NaCl, 1% NP40, 5% glycerol, 5 mM $MgCl_2$). GST pull-downs were resuspended in 2×loading buffer for SDS/PAGE analysis.

Recombinant protein production

The cDNAs encoding for His-tagged *KRAS*, *RGS3* and *NF1* GRD were cloned into the pET28a expression vector and expressed in *E. coli* BL21 (DE3) cells. Protein expression was induced by adding 0.5 mM isopropyl β-D-thiogalactopyranoside (IPTG) in Terrific Broth medium at 16 °C for 18 h. Bacterial cells were harvested and then resuspended with lysis buffer (20 mM HEPES, pH 7.5, 500 mM NaCl, 5% glycerol, 1 mM DTT, and 20 mM imidazole). The cell debris was removed by centrifugation at 16,000 rpm for 60 min at 4 °C, and the soluble fraction was loaded onto nickel-sepharose (GE Healthcare) pre-equilibrated with lysis buffer. After sequential washes with lysis buffer containing 20 mM and then 40 mM imidazole, the proteins were eluted with lysis buffer containing 400 mM imidazole. The target proteins were further purified by size-exclusion chromatography in a Superdex 200 column (GE Healthcare) in buffer containing 20 mM HEPES, pH 7.5, 150 mM NaCl, and 1 mM DTT.

GST-tagged KRAS or RGS3 GAP domain were cloned in the pGEX-4T-1 expression vector and expressed in *E. coli* BL21(DE3) cells. Protein expression was induced by adding 0.5 mM IPTG as above. Bacterial cells were harvested and then resuspended with phosphate-buffered saline (PBS) before being lysed. The cell debris was removed by centrifugation at 16,000 rpm for 60 min at 4 °C, and the soluble fraction was loaded onto glutathione-sepharose (GE Healthcare) pre-equilibrated with PBS. After washing with PBS, proteins were eluted with 10 mM glutathione, 50 mM Tris-HCl, pH 8.0. The target proteins were further purified by size-exclusion chromatography as above.

Molecular modeling

Protein-protein docking was carried out in a heuristic manner using the tools in Maestro/Bioluminate (Schrodinger), as described by the manufacturer. Briefly, the model was based on several existing structures, including KRAS-GMPPNP (6OB2) and RGS3 GAP domain (2OJ4). Superimposition of the structure of KRAS to that of Ga_{ia1} (1AGR) revealed a similar architecture of the key motifs responsible for GTP-hydrolysis (i.e., the P-loop, switch I and switch II regions show a high degree of overlap between the two proteins). Based on this observation, the structure of Gia1-GDP·AlF4:RGS4 (1AGR) was used to define several anchoring points and refine

the docking poses for KRAS-RGS3. Known contacts between RGS4 and Gia1 were used as docking constraints. Prior to protein-protein docking, the structures of KRAS-GMPPNP and RGS3 GAP domain were prepared by adding hydrogens, assigning bond orders, creating disulfide bonds, adding missing side chains, deleting waters beyond 5Å, assigning H-bonds and restraining minimization. These were carried out using the protein-preparation wizard in Maestro and default settings. Priority was given to poses satisfying the constraints noted above. Since we were most interested in identifying residues that could potentially mediate the GAP activity of RGS3 on KRAS, initial poses were manually evaluated to identify potential residues that might enhance hydrolysis and not be impeded by G12 substitutions. This initial approach, coupled with evidence from the literature, suggested a potential role for an asparagine residue in RGS3 GAP domain. Once the importance of this residue was confirmed experimentally the docking was repeated with more stringent constraints around this residue.

RGS3 knockout

H358 cells were transiently transfected with a plasmid (pSpCas9-2A) encoding RGS3-specific sgRNAs. Two different sgRNA were used: sgRGS3#1: TGCGTGATCCTCTTCCTGGC; sgRGS3#2: CTACACGCGGGAGCACACCA. After 48h, GFP-positive cells were FACS-sorted into 96 well plates, with a single cell per well. Each cell was allowed to expand into a clone, these were then expanded and screened for RGS3 deletion by Sanger sequencing and immunobloting using a monoclonal antibody detecting RGS3.

Live-Cell Analysis

Control or RGS3-null H358 cells were seeded at 10–20% confluence in a 24 well-plate and transfected with 5 pmol of non-targeting (NT) or $KRAS^{G12C}$-specific siRNA (siG12C) *(17)*. H358 cells expressing G12C or G12C/A59G mutant KRAS were seeded at 10–20% confluence and transfected with 5 pmol of non-targeting (NT) or RGS3-specific siRNA (Horizon, L-008302-01-0010). Images of cell confluence were automatically acquired within Incucyte (Essen BioScience). The images were taken at 2 h intervals for the duration of the experiment. The % confluence was determined by using the Incucyte software (Essen BioScience).

3D tumor spheroid assays

Cells were added at a density of 4×10^3 cells/mL in a solution containing collagen I (A1048301, Gibco) at a final concentration of 2 mg/mL. The collagen-cell mixture (300 µL) was then added to collagen I pre-coated 35 mm dishes. The mixture was incubated for 30 min at 37°C, followed by addition of 2 mL culture medium and incubation for the indicated days in a 37°C, 5% CO2 incubator. Spheroids were imaged using an Inverted Research Microscope Ti2 (Nikon) and their data were analyzed using NIS-Elements.

Immunohistochemistry analysis

The tissue sections from paraffin-embedded PDX tumors were stained with RGS3 antibody. We quantitatively scored the tissue sections according to the percentage of positive cells and staining intensity. IHC images were quantified in an automated manner by using the QuPath software (University of Edinburgh, Division of Pathology) *(35)*. The score (*H*-score) was obtained using the formula: $X3 + 2 \times X2 + 3 \times X1$ giving a range of 0 to 300 ($0 \leq [X1 + X2 + X3] \leq 100$), where $X3$ indicates weak staining, $X2$ moderate staining and $X1$ strong staining. The H-score was correlated with pattern of G12Ci-response.

Correlation of RGS3 expression with KRAS mutant transcriptional output

The lung adenocarcinoma TCGA RNAseq dataset was obtained from the Genomic Data Commons Data Portal as HT-Seq counts. Count data were filtered and normalized using edgeR and standard approaches. Genes with an absolute log fold change in expression of greater than 1 and an FDR of less than 0.05 in the KRAS mutant vs. wild-type tumor comparison were used to establish a mutant KRAS output score. The latter was defined as the mean log-transformed normalized (count per million) expression of up- or down-regulated genes. The ability of this score to determine changes in KRAS signaling was experimentally validated in H358 cells treated with a G12C inhibitor over time (0-48h, fig. S8C).

The correlation between mutant KRAS output score and RGS3 expression was determined by two approaches. In the first approach, RGS3 expression in log counts per million was categorized as low (< 0.25 percentile), intermediate (0.25-0.75 percentile) and high (> 0.75 percentile) across the entire dataset. The distribution of KRAS-up scores along these categories, both in KRAS wild-type and in KRAS mutant lung cancers, were compared using ANOVA and Turkey tests, while correcting for multiple comparison testing. In the second approach, the correlation between RGS3 expression (log count per million, continuous variable) and mutant KRAS output score (up or down) were determined by using the Spearman coefficient.

Animal studies

This was carried out as described previously *(36)*. Briefly, nu/nu athymic mice were obtained from the Envigo Laboratories and maintained in compliance with IACUC guidelines under protocol 18-05-007 approved by MSKCC IACUC. The maximum tumor measurement permitted was 1.5 cm in diameter and this was not exceeded in any of our experiments. Animals implanted with xenografts were chosen for efficacy studies in an unbiased manner. Once tumors reached 100 mm^3 volume, mice were randomized and treated with drug or the appropriate vehicle control. Treatments and tumor measurements were performed in a non-blinded manner by a research technician who was not aware of the objectives of the study. Prism (GraphPad Software Inc.) was used for data analysis. For each study arm, the tumor size was plotted over time. Statistically significant differences were determined for endpoint tumor volumes (Fig. 4B and C) or for the fractional difference in tumor change relative to baseline (fig. S9D) by the t-test function embedded in Prism (unpaired, two-tailed). In these comparisons, the two control sgRNAs (each n=5) were pooled together. As an alternative, each sgRGS3 clone in Fig. 4C was compared to a separate non-targeting sgRNA-expressing control clone. For the latter, fractional differences in tumor growth relative to baseline were compared using the multiple unpaired t-test function (one t test per time point) in Prism and corrected for multiple hypothesis testing by using the false discovery rate (FDR) approach. The $RGS3^{-/-}$ clone 2.5 vs control 1 comparison reached statistical significance (FDR q value <0.05) on days 35-42 for the 10 mpk treatment condition and on day 42 for the 50 mpk condition. The $RGS3^{-/-}$ clone 3.1 vs control 2 comparison did not reach significance during the course of the experiment for the 10 mpk condition but reached significance on days 20-42 for the 50 mpk condition. The data from control clones were grouped together in graphs in order to simplify visualization.

Supplementary text

Here we report that RGS3 acts as a mutant KRAS-inclusive GAP to enhance GTP hydrolysis by both wild-type and several G12/G13 mutant KRAS. The effect of RGS3 was dependent on an asparagine residue in its GAP domain — unlike the catalytic arginine finger of canonical RAS-GAPs. Several findings support the possibility that other cellular proteins have a similar activity as that observed for RGS3. RGS3-null extracts retained some GTPase enhancing activity directed at $KRAS^{G12C}$. Other RGS family members contain the key asparagine residue and are reported to have redundant roles in G-protein coupled receptor (GPCR) signaling. Indeed, RGS4 also enhanced GTP hydrolysis by $KRAS^{G12C}$. Even NF1 had some activity directed at $KRAS^{G12C}$ in biochemical assays and has been shown to inactivate $KRAS^{G13D}$ in biochemical and cellular studies *(26)*. In our experiments, the $KRAS^{G12C}$-directed activity of NF1 was independent of the R-finger. Together these observations suggest that GTP-hydrolysis by common oncogenic KRAS mutants is enhanced by atypical, non R-finger dependent, GAPs.

KRAS mutations at Q61, which are much less frequent than those occurring at G12 or G13, render KRAS insensitive to GAP-assisted hydrolysis by impairing the coordination of the water molecule needed for nucleophilic attack on the ɣ-phosphate. However, it was recently shown that direct suppression of the guanine-nucleotide exchange factor (GEF) SOS1 inhibited proliferation in some KRAS Q61 mutant driven cells *(37)*. This finding suggests that not all Q61 mutants are deficient in hydrolysis in cells. More work is needed to systematically characterize the susceptibility of less frequent KRAS mutants (such as Q61 or other) to RGS3- or atypical GAP-assisted hydrolysis.

Previous work shows that cellular lysates enhance the GTPase activity of wild-type RAS but not that of mutant RAS *(5)*. These seminal studies focused predominantly on NRAS and HRAS and the mutants commonly tested were G12V or G12D. To our knowledge, the effect of cell extracts on $KRAS^{G12C}$ has not been previously tested. Nevertheless, our data agree that mutant KRAS has impaired GTPase activity relative to $KRAS^{WT}$. We only differ in the magnitude of impairment. The historical model suggests that mutant RAS is completely unresponsive to cellular GAPs. We now postulate that $KRAS^{G12C}$ is sensitive to cellular GAPs; albeit much less so than $KRAS^{WT}$.

We believe that the difference in sensitivity lies on the mechanism responsible for the enhanced GTPase activity by cellular extracts. For $KRAS^{WT}$ the activity is mediated by canonical RAS-GAPs, such as NF1 and RASA1, in an arginine-dependent manner. This process is very fast, reaching steady state in a matter of seconds. For $KRAS^{G12C}$ the activity is mediated by atypical GAPs, through a process that is faster than intrinsic hydrolysis but ~1-2 orders of magnitude slower than the activity of canonical GAPs towards $KRAS^{WT}$. In other words, RGS3 is a weaker GAP for $KRAS^{G12C}$ than NF1 is for $KRAS^{WT}$, a finding with two important implications: a) Despite enhancing GTP hydrolysis by $KRAS^{WT}$ in biochemical assays, RGS3 is unlikely to regulate $KRAS^{WT}$ in cells, unless canonical GAPs are inactivated. Indeed, RGS3-null extracts did not enhance the GTPase activity of $KRAS^{G12C}$ but did so towards $KRAS^{WT}$. Also, RGS3 interacted with $KRAS^{G12C}$ but not $KRAS^{WT}$ in cells. b) RGS3 is unlikely to inactivate the entire cellular pool of mutant KRAS; that is, not to the same extent as NF1/RASA1 are able to do for wild-type KRAS. Therefore, under steady-state conditions, the nucleotide cycle of mutant KRAS favors the active state, whereas that of wild-type KRAS favors the inactive state. Our model thus provides a mechanistic basis for how KRAS mutants drive tumor growth, while at the same time remaining

susceptible to atypical GAP-assisted hydrolysis. The model also helps explain the susceptibility to inactive state selective inhibition and the dependency of various KRAS oncoproteins on nucleotide-exchange for their activation.

As expected, RGS3 deletion led to enhanced KRAS activation and tumor growth as well as diminished inactive state selective $KRAS^{G12C}$ inhibition. Although the RGS3-null phenotypes may occur via an effect on Gα, several lines of evidence suggest a dependency on $KRAS^{G12C}$. Selective knockdown of $KRAS^{G12C}$ reversed the phenotype of RGS3-null cells, whereas knockdown of RGS3 enhanced the growth of $KRAS^{G12C}$-expressing cells but not that of $KRAS^{G12C/A59G}$-expressing cells. Furthermore, RGS3-depleted cell extracts had a diminished GTPase-enhancing effect towards $KRAS^{G12C}$, as compared to RGS3 wild-type extracts. The activity was restored in RGS3-null cells expressing $RGS3^{WT}$ but diminished again in cells expressing $RGS3^{N460H}$. In a similar manner, the increase in cellular KRAS activation and proliferation caused by RGS3 deletion was rescued by $RGS3^{WT}$ but not by $RGS3^{N460H}$. Lastly, extracts from RGS3-null cells did not significantly affect GTP[γ^{32}P] hydrolysis by $KRAS^{WT}$. If the effects were non-specific then RGS3-null lysates would have also affected $KRAS^{WT}$. Together, these lines of evidence support the conclusion that in the biological context of our study, the consequences of RGS3 deletion are, at least in part, due to an effect on $KRAS^{G12C}$. While we do not dismiss a potential contribution by Ga signaling, the latter does not appear to be dominant in the context of our experimental data.

Our work suggests that atypical GAP-assisted hydrolysis and nucleotide exchange jointly coordinate the nucleotide cycle of mutant KRAS to regulate its activation in cancer cells. Negative and positive feedback circuits are likely to further fine tune these processes. With these in mind, it is possible that the expected cellular effects of RGS3 deletion (including the increase of KRAS-GTP levels and proliferation) are blunted over time by compensatory effects in GEF-mediated nucleotide exchange. Moreover, other RGS family members or other non R-finger GAPs may compensate for the loss of RGS3. Future studies are necessary in order to better understand the dynamics of atypical GAP-assisted mutant KRAS hydrolysis and its interplay with nucleotide exchange and feedback.

Although RGS3 was required for maximal inactive state selective $KRAS^{G12C}$ inhibition, the compensatory changes noted above are likely to modulate this effect as well. For example, loss of RGS3 leads to enhanced KRAS-GTP levels, which is expected to attenuate inhibition by decreasing the pool of drug-sensitive target. Over time, however, a feedback-mediated compensatory decrease in nucleotide exchange might enable sufficient drug binding to the target especially for high-affinity inhibitors. Dedicated studies are needed to understand if and how RGS3 (and/or other atypical GAPs) correlate with adaptive, acquired or de-novo resistance in experimental models and patients.

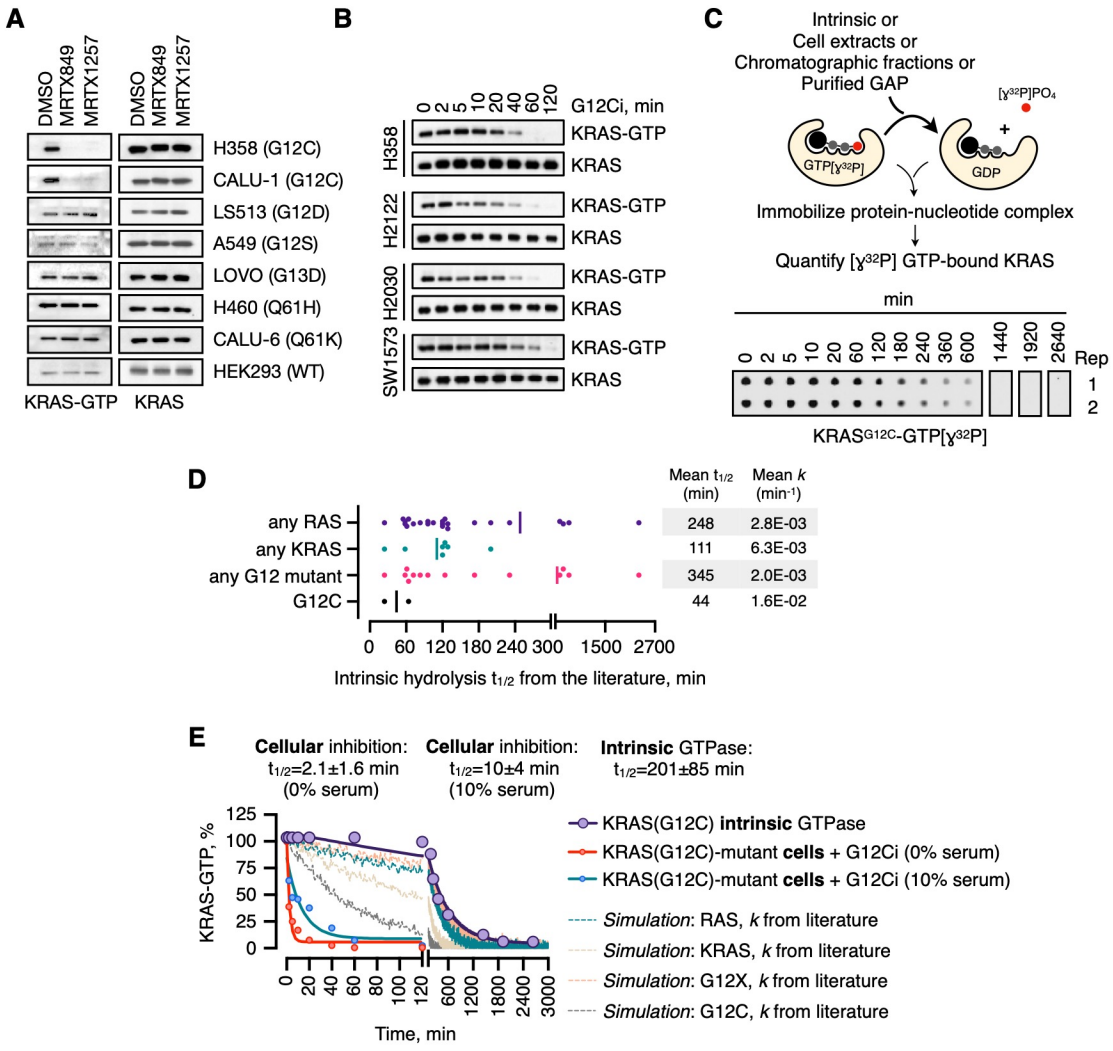

Fig. S1. Cellular KRAS^{G12C} inhibition is faster than its intrinsic hydrolysis rate. (**A**) WCE from cancer cell lines treated with the indicated G12Ci (500 nM) for 2h were subjected to RBD-pull down to determine the level of active KRAS. (**B**) KRAS^{G12C}-mutant cells were treated in complete medium containing a MRTX1257 (500 nM). (**C**) Schematic of the ɣ-phosphate assay used to measure the GTPase activity of KRAS. Bottom: purified KRAS^{G12C} was loaded with GTP[ɣ^{32}P] and assayed to determine its intrinsic GTPase activity over time. Rep: biological replicate. (**D**) Intrinsic hydrolysis half-lives ($t_{1/2}$) and rate constants (*k*) from the literature. (**E**) KRAS pulldowns were quantified by densitometry and analyzed to determine the half-life for cellular inhibition by MRTX1257 (mean ± s.e.m, n=4). The dotted lines represent simulated data using mean rate constants from the literature.

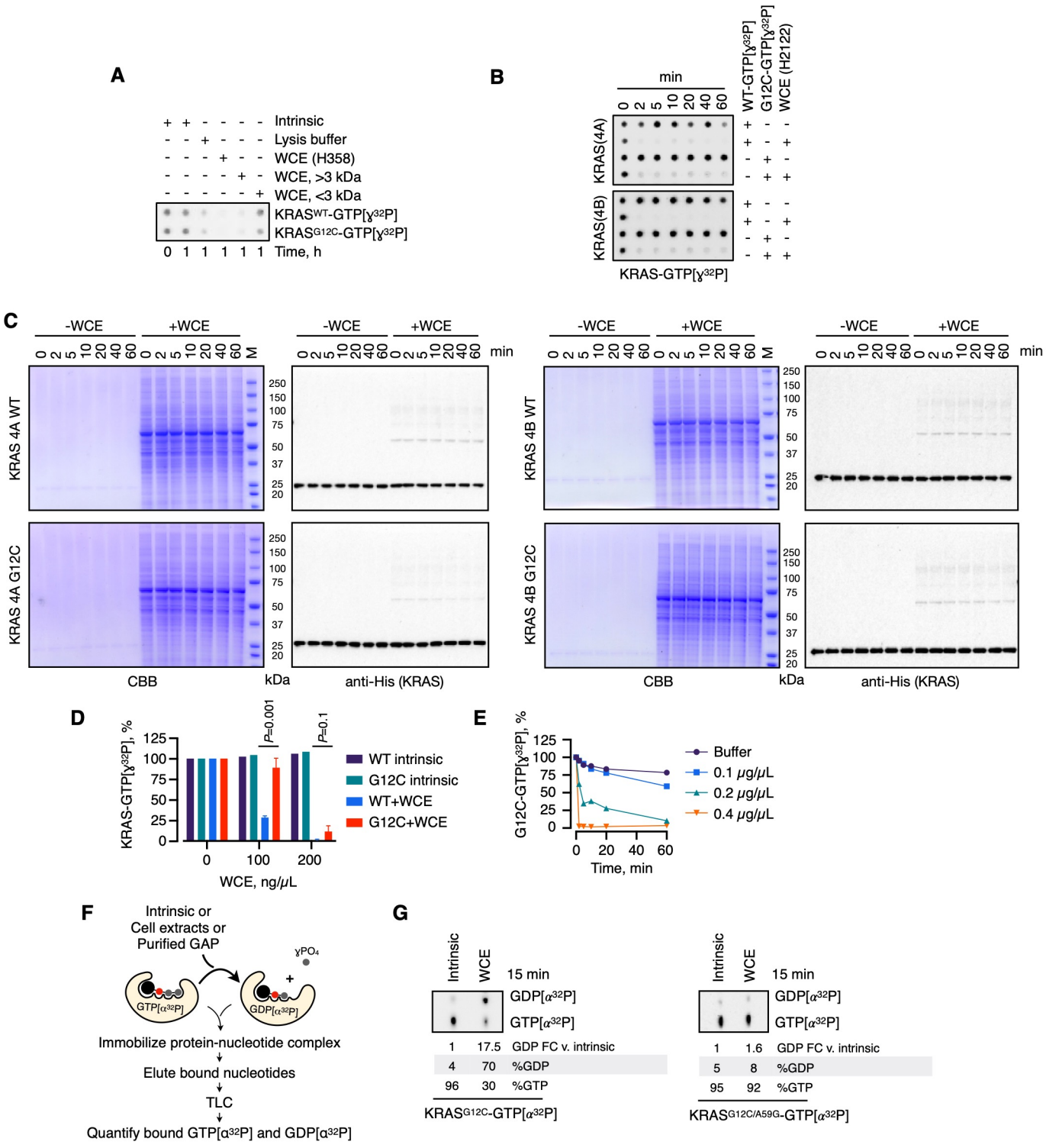

Fig. S2. KRAS^{G12C}-directed GTPase-enhancing activity in cell extracts. (**A**, **B**) GTP[γ^{32}P] hydrolysis was assayed in the absence or presence of WCE from the indicated cancer models. The effect of cellular lysate fractionation with a 3 kDa molecular cut-off column is shown in A. The effect on KRAS 4A and 4B splice variants over time is shown in B. A representative of at least two experimental repeats is shown. (**C**) The indicated His-tagged KRAS variants were purified, loaded with GTP[γ^{32}P], and subjected to GTPase assays in the absence or presence of cellular extracts. The reactions were subjected to SDS-PAGE followed by Coomassie Brilliant Blue (CBB) staining or immunoblotting with a His-specific antibody. M: molecular weight marker. (**D**, **E**) Purified KRAS^{WT} and/or KRAS^{G12C} were loaded with GTP[γ^{32}P] and assayed for hydrolysis in the presence of WCE at 2 min (D) or over time (E). (**F**) Schematic of the *α*-phosphate hydrolysis assay. TLC: thin layer chromatography. (**G**) The indicated KRAS variants were analyzed as shown in F.

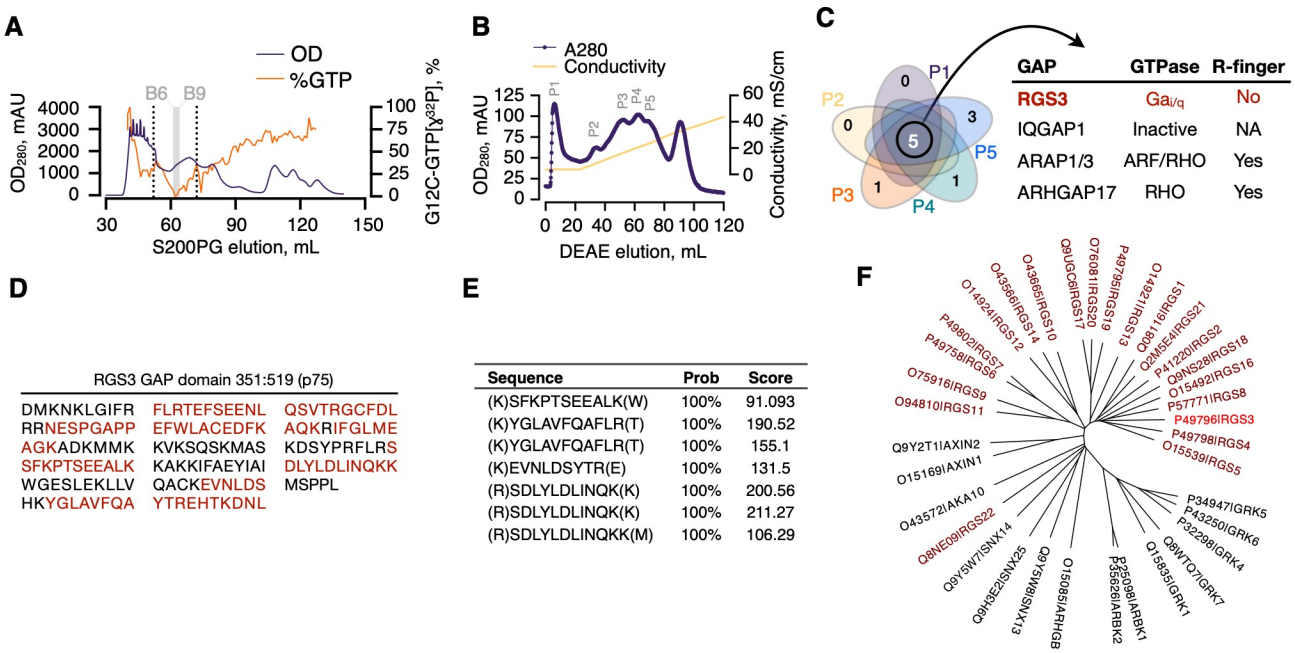

Fig. S3. Identification of RGS3 during chromatographic analysis. (**A**) H358 cell extracts (2 g) were subjected to SEC (step 1). Eluted fractions (1 mL each) were incubated with GTP[γ^{32}P]-loaded KRAS^{G12C} for 1 h and subjected to the γ-phosphate hydrolysis assay. The optical density (OD, 280 nm) and the % GTP[γ^{32}P] signal in each fraction are shown. (**B**) Active fractions from SEC step 2 (12-17 mL, see Fig. 2A) were pooled, desalted (step 3) and subjected to AEC using a linear salt-gradient (step 4). The conductivity and optical density are shown. See Fig. 2C for the effect of each fraction on GTPase activity. (**C**) Fractions with enhanced GTPase activity (P1-5) in AEC (step 4) were pooled, proteins were acid-precipitated and subjected to mass spectrometry for identification of proteins annotated as GAP. (**D**, **E**) The mass spectrometry sequence coverage of the RGS3 GAP domain (RGSD, D) as well as the score corresponding to several identified peptides (E) are shown. Residue numbering in C is from P49796-1 (Uniprot). (**F**) Phylogenetic tree of 35 human RGS domain-containing proteins, based on their primary protein sequence similarity. Red text denotes RGS family members, bright red text denotes RGS3, black text denotes other proteins containing an RGS GAP domain.

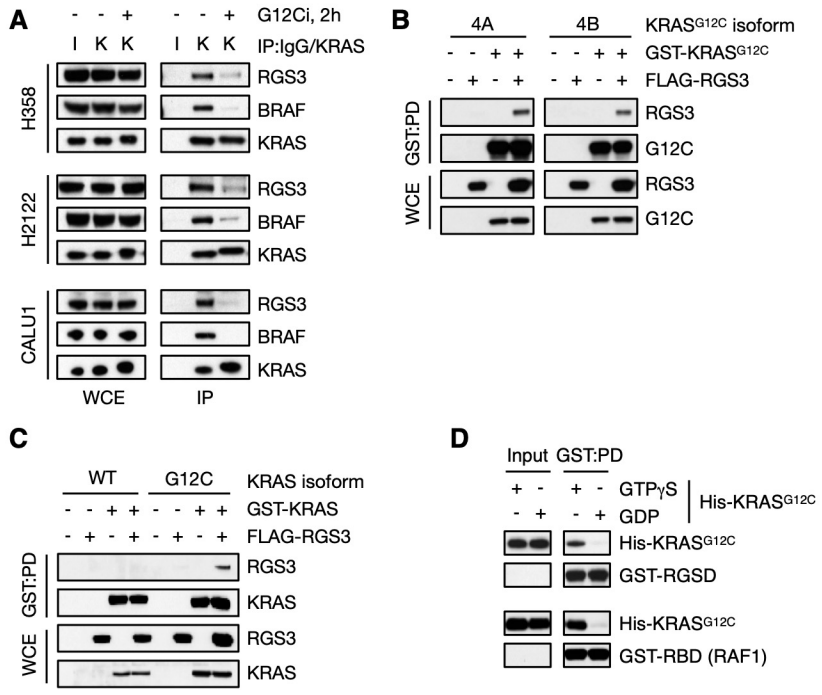

Fig. S4. RGS3 interacts with KRAS^{G12C} in a nucleotide-dependent manner. (**A**) Co-immunoprecipitation (IP) of endogenous KRAS and RGS3 from KRAS^{G12C}-mutant cell lines treated as shown. BRAF is included as an internal control. I: IgG antibody agarose-conjugate, K: KRAS antibody agarose-conjugate. (**B**, **C**) HEK293 cells expressing FLAG-RGS3 in combination with the indicated KRAS splice variants (B) or with wild-type or mutant KRAS (C) were subjected to a GST-pulldown. (**D**) His-tagged purified KRAS^{G12C} was loaded with non-hydrolyzable GTPγS or GDP. Top: The proteins were incubated with purified GST-RGS domain (RGSD) and subjected to GST-pulldown to determine the presence of an interaction. Bottom: A pulldown with the RAS-binding domain (RBD) or RAF1, which is known to selectively interact with GTP-bound RAS, was used as a control. A representative of at least two experimental repeats is shown in A-D.

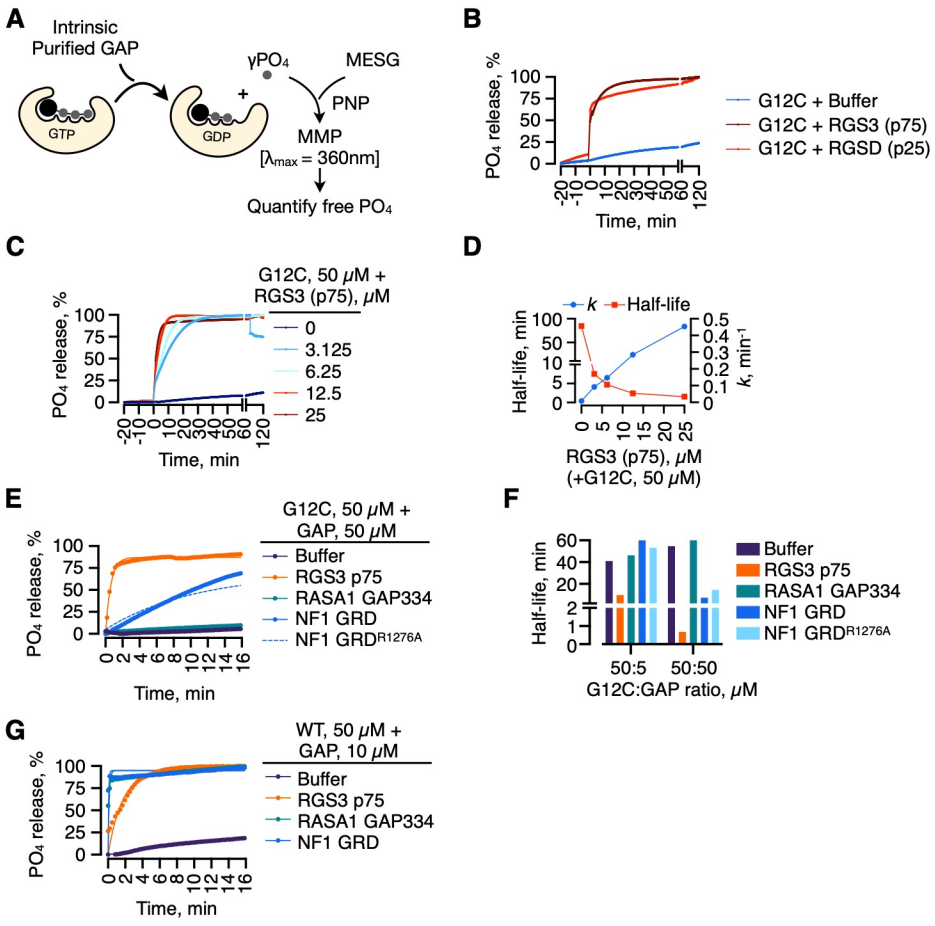

Fig. S5. RGS3 enhances GTP hydrolysis by G12C mutant and wild-type KRAS. (**A**) Schematic of the continuous γ-PO_4 release assay used to measure the GTPase activity of KRAS. MESG: 2-amino-6-mercapto-7-methylpurine riboside, PNP: purine nucleoside phosphorylase, MMP: ribose 1-phosphate and 2-amino-6-mercapto-7-methylpurine. (**B**, **C**) GTP-loaded KRAS variants were desalted and incubated at room temperature with buffer or the RGS proteins shown in the presence of MESG and PNP. KRAS and RGS3 were incubated at a an equimolar ratio (50 μM, B) or as indicated (C). The GAP was added just before 0 min. (**D**) The half-life and rate constant (*k*) for the RGS-assisted $KRAS^{G12C}$ GTP-hydrolysis were determined by fitting a one-phase association curve to the data (0-60 min). (**E-G**) GTP-loaded $KRAS^{G12C}$ (E, F) or $KRAS^{WT}$ (G) was reacted with RGS3, RASA1 or NF1 at the indicated molar ratios. NF1 mutated at the catalytic R-finger was also assayed. The kinetic profile is shown in E and the reaction half-life in F. A representative of two experimental repeats is shown in B, C and E.

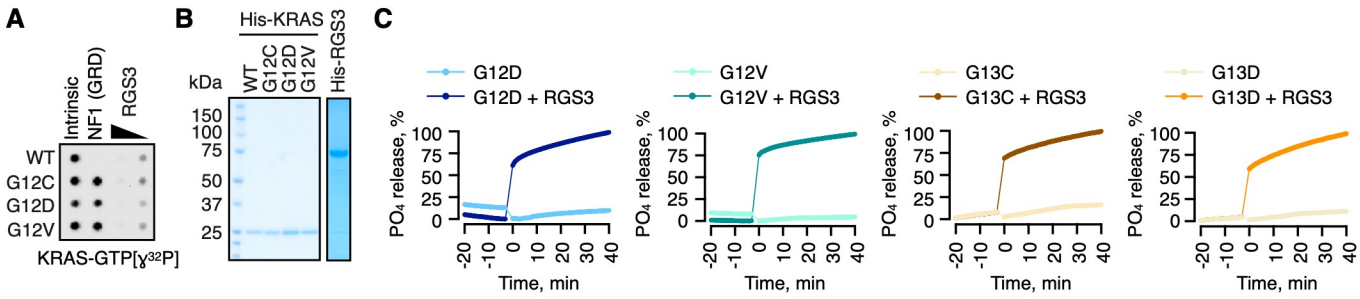

Fig. S6. RGS3 enhances GTP-hydrolysis by several G12/G13 KRAS mutants. (**A**) The indicated G12 mutant KRAS oncoproteins were loaded with GTP[γ^{32}P] and assayed for GTP hydrolysis in the presence of NF1 (GRD) or RGS3 (p75). (**B**) The purity of the protein preparation was determined by CBB staining. (**C**) The indicated GTP-loaded KRAS variants were subjected to hydrolysis assay either alone or in the presence of RGS3 (25 μM each).

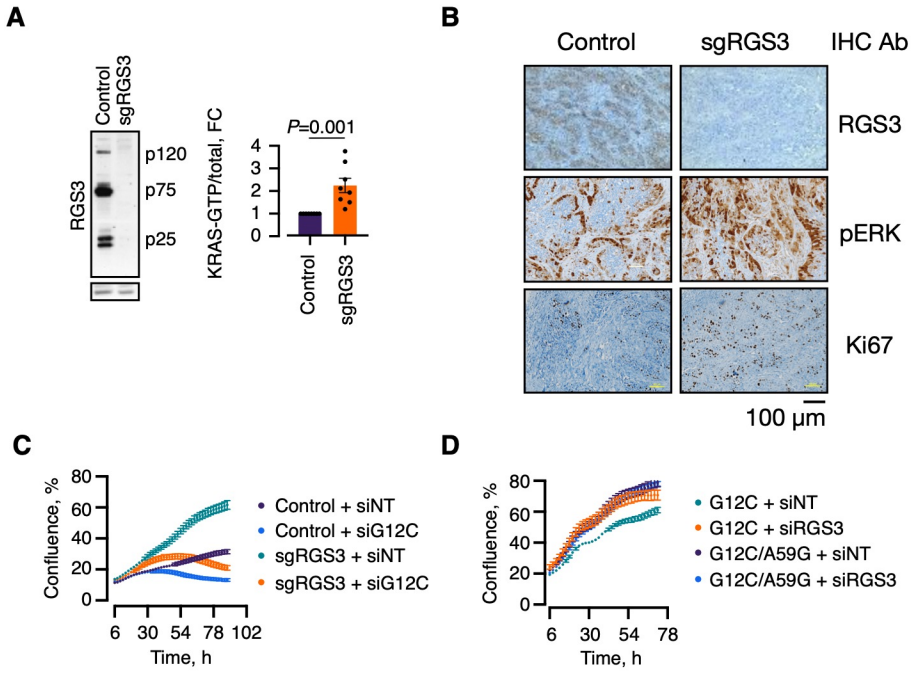

Fig. S7. Effect of RGS3 loss on KRAS activation and proliferation. (**A**) WCE from H358 cells expressing control of RGS3-specific sgRNAs were immunoblotted to determine RGS3 expression or subjected to RBD-pulldown to determine the effect on active (GTP-bound) KRAS (mean ± s.e.m, n=7, two tailed p value). (**B**) Tumors from mice bearing control or RGS3-null xenografts were subjected to immunohistochemistry (IHC) as shown. (**C**) Control or RGS3-null cells were transfected with a non-targeting (NT) or a $KRAS^{G12C}$-specific siRNA. The effect on cell proliferation (% confluence) was determined by continuous monitoring using Incucyte. (**D**) H358 cells expressing G12C- or G12C/A59G-mutant KRAS were transfected with control or RGS3-specific siRNAs to determine the effect on proliferation over time.

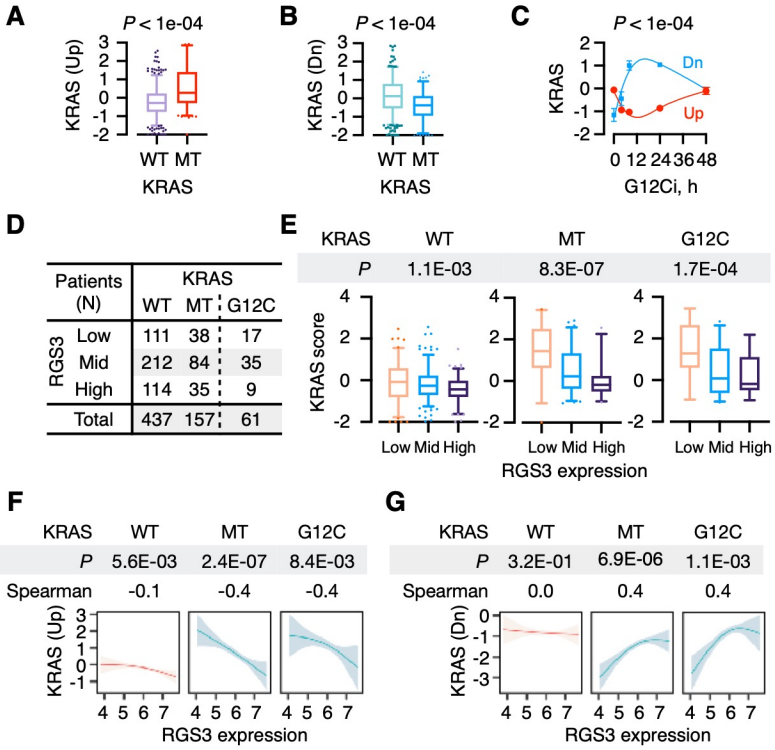

Fig. S8. RGS3 expression inversely correlates with mutant KRAS transcriptional output in patients. (**A**, **B**) RNAseq from the lung adenocarcinoma TCGA dataset was used to determine differentially expressed genes between KRAS mutant and wild-type cancers. The KRAS activation score was derived from the mean normalized expression of distinct up- (A) or down- (B) regulated genes and scaled across samples. Median, upper/lower quantiles and outliers as well as two-tailed p values are shown. Dn: down. **(C)** Validation of the KRAS score in $KRAS^{G12C}$-mutant (H358) cells treated with a G12Ci over time. (**D**) Contingency table of patients with lung cancer used to correlate RGS3 expression with mutant KRAS-driven transcriptional output. (**E**) KRAS activation score in lung cancers with low, mid and high RGS3 expression (categorized). ANOVA p values are shown. **(F**, **G**) The correlation coefficient between normalized RGS3 expression (continuous) and up-regulated (F) or down-regulated (G) KRAS activation scores in lung cancers with wild-type or mutant KRAS.

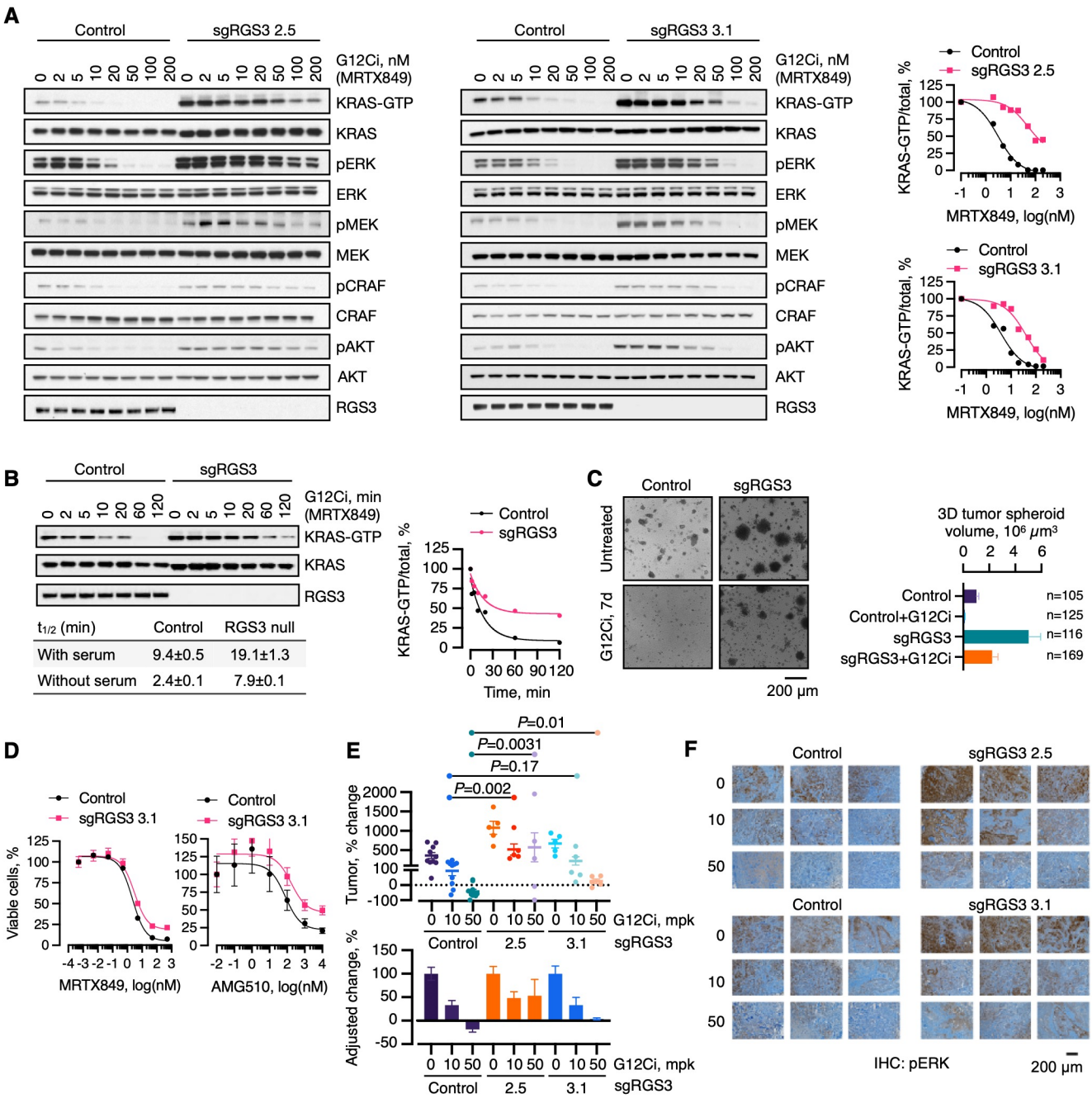

Fig. S9. RGS3 is required for maximal inactive state-selective KRAS^{G12C} inhibition. (**A**) Control or RGS3$^{-/-}$ cells were treated with increasing concentrations of MRTX849 in serum free medium and assayed to determine the effect on KRAS activation or downstream signaling intermediates. Total and GTP bound KRAS levels were quantified by using densitometry and plotted on the right. (**B**) As in A but the cells were treated with MRTX849 (500 nM) in complete medium. (**C**) The indicated cells were cultured as 3D tumor spheroids in collagen I-containing medium for 14 days, either in the absence or presence of G12Ci (500 nM). Shown are representative images (left) and spheroid volumes (right, mean ± s.e.m). (**D**) The indicated cell lines were treated as shown for 72 h to determine the effect on cell viability by ATP-glow. (**E**) As in Fig. 4C, but the percent in tumor change at endpoint relative to d0 was used to compare tumor growth inhibition. Two tailed p values are shown. The bottom graph shows the adjusted change relative to the vehicle-treated condition (0) for each group. (**F**) Sections from the indicated tumors were subjected to IHC with a pERK specific antibody. Three representative images for each condition are shown.

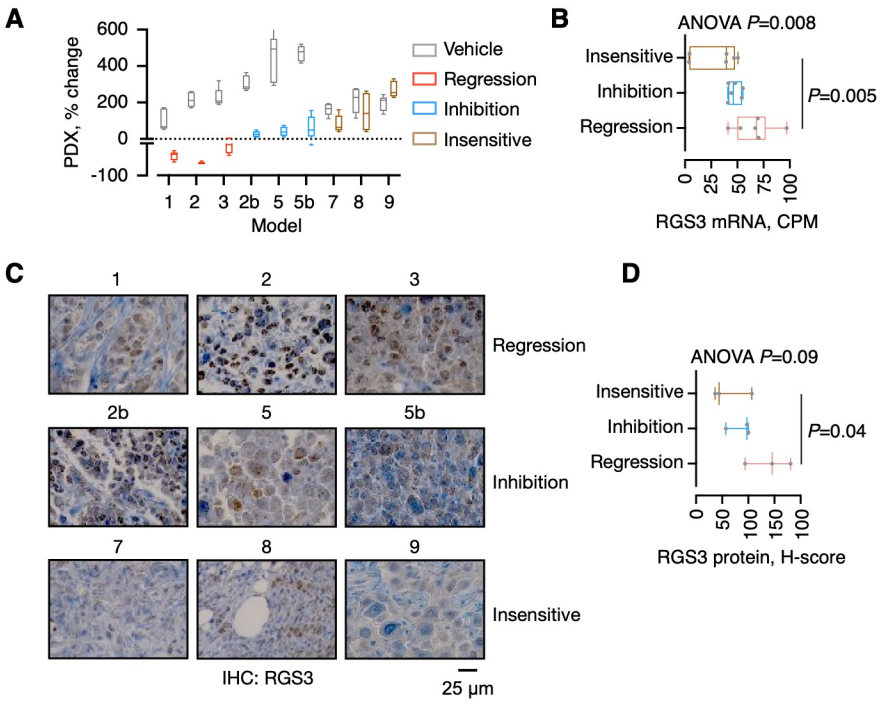

Fig. S10. RGS3 expression correlates with G12Ci sensitivity in patient-derived xenografts. (**A**) Mice bearing KRAS^{G12C}-mutant lung cancer PDX models were treated with vehicle or MRTX1257 (50 mg/kg). The best treatment response in each model is shown (n=4 per group). (**B**) Representative vehicle-treated tumors from A (2 tumors per PDX) were subjected to RNA sequencing to determine the expression of RGS3 and its correlation with response. (**C**) Representative images of vehicle treated PDX tumors subjected to IHC with an RGS3-specific antibody. (**D**) IHC images were quantified using QuPath and the H-score was correlated with pattern of G12Ci-response. ANOVA and group-specific comparison p values are shown in B and D.

References and Notes

1. M. Malumbres, M. Barbacid, RAS oncogenes: The first 30 years. *Nat. Rev. Cancer* **3**, 459–465 (2003). doi:10.1038/nrc1097 Medline

2. B. Papke, C. J. Der, Drugging RAS: Know the enemy. *Science* **355**, 1158–1163 (2017). doi:10.1126/science.aam7622 Medline

3. D. K. Simanshu, D. V. Nissley, F. McCormick, RAS proteins and their regulators in human disease. *Cell* **170**, 17–33 (2017). doi:10.1016/j.cell.2017.06.009 Medline

4. S. Li, A. Balmain, C. M. Counter, A model for RAS mutation patterns in cancers: Finding the sweet spot. *Nat. Rev. Cancer* **18**, 767–777 (2018). doi:10.1038/s41568-018-0076-6 Medline

5. M. Trahey, F. McCormick, A cytoplasmic protein stimulates normal N-ras p21 GTPase, but does not affect oncogenic mutants. *Science* **238**, 542–545 (1987). doi:10.1126/science.2821624 Medline

6. S. M. Margarit, H. Sondermann, B. E. Hall, B. Nagar, A. Hoelz, M. Pirruccello, D. Bar-Sagi, J. Kuriyan, Structural evidence for feedback activation by Ras.GTP of the Ras-specific nucleotide exchange factor SOS. *Cell* **112**, 685–695 (2003). doi:10.1016/S0092-8674(03)00149-1 Medline

7. J. L. Bos, H. Rehmann, A. Wittinghofer, GEFs and GAPs: Critical elements in the control of small G proteins. *Cell* **129**, 865–877 (2007). doi:10.1016/j.cell.2007.05.018 Medline

8. Y. Pylayeva-Gupta, E. Grabocka, D. Bar-Sagi, RAS oncogenes: Weaving a tumorigenic web. *Nat. Rev. Cancer* **11**, 761–774 (2011). doi:10.1038/nrc3106 Medline

9. G. Bollag, F. McCormick, Differential regulation of rasGAP and neurofibromatosis gene product activities. *Nature* **351**, 576–579 (1991). doi:10.1038/351576a0 Medline

10. K. Scheffzek, M. R. Ahmadian, W. Kabsch, L. Wiesmüller, A. Lautwein, F. Schmitz, A. Wittinghofer, The Ras-RasGAP complex: Structural basis for GTPase activation and its loss in oncogenic Ras mutants. *Science* **277**, 333–338 (1997). doi:10.1126/science.277.5324.333 Medline

11. J. M. Ostrem, U. Peters, M. L. Sos, J. A. Wells, K. M. Shokat, K-Ras(G12C) inhibitors allosterically control GTP affinity and effector interactions. *Nature* **503**, 548–551 (2013). doi:10.1038/nature12796 Medline

12. P. Lito, M. Solomon, L. S. Li, R. Hansen, N. Rosen, Allele-specific inhibitors inactivate mutant KRAS G12C by a trapping mechanism. *Science* **351**, 604–608 (2016). doi:10.1126/science.aad6204 Medline

13. M. P. Patricelli, M. R. Janes, L.-S. Li, R. Hansen, U. Peters, L. V. Kessler, Y. Chen, J. M. Kucharski, J. Feng, T. Ely, J. H. Chen, S. J. Firdaus, A. Babbar, P. Ren, Y. Liu, Selective inhibition of oncogenic KRAS output with small molecules targeting the inactive state. *Cancer Discov.* **6**, 316–329 (2016). doi:10.1158/2159-8290.CD-15-1105 Medline

14. M. R. Janes, J. Zhang, L.-S. Li, R. Hansen, U. Peters, X. Guo, Y. Chen, A. Babbar, S. J. Firdaus, L. Darjania, J. Feng, J. H. Chen, S. Li, S. Li, Y. O. Long, C. Thach, Y. Liu, A. Zarieh, T. Ely, J. M. Kucharski, L. V. Kessler, T. Wu, K. Yu, Y. Wang, Y. Yao, X. Deng,

P. P. Zarrinkar, D. Brehmer, D. Dhanak, M. V. Lorenzi, D. Hu-Lowe, M. P. Patricelli, P. Ren, Y. Liu, Targeting KRAS mutant cancers with a covalent G12C-specific inhibitor. *Cell* **172**, 578–589.e17 (2018). doi:10.1016/j.cell.2018.01.006 Medline

15. J. Canon, K. Rex, A. Y. Saiki, C. Mohr, K. Cooke, D. Bagal, K. Gaida, T. Holt, C. G. Knutson, N. Koppada, B. A. Lanman, J. Werner, A. S. Rapaport, T. San Miguel, R. Ortiz, T. Osgood, J.-R. Sun, X. Zhu, J. D. McCarter, L. P. Volak, B. E. Houk, M. G. Fakih, B. H. O'Neil, T. J. Price, G. S. Falchook, J. Desai, J. Kuo, R. Govindan, D. S. Hong, W. Ouyang, H. Henary, T. Arvedson, V. J. Cee, J. R. Lipford, The clinical KRAS(G12C) inhibitor AMG 510 drives anti-tumour immunity. *Nature* **575**, 217–223 (2019). doi:10.1038/s41586-019-1694-1 Medline

16. J. Hallin, L. D. Engstrom, L. Hargis, A. Calinisan, R. Aranda, D. M. Briere, N. Sudhakar, V. Bowcut, B. R. Baer, J. A. Ballard, M. R. Burkard, J. B. Fell, J. P. Fischer, G. P. Vigers, Y. Xue, S. Gatto, J. Fernandez-Banet, A. Pavlicek, K. Velastagui, R. C. Chao, J. Barton, M. Pierobon, E. Baldelli, E. F. Patricoin 3rd, D. P. Cassidy, M. A. Marx, I. I. Rybkin, M. L. Johnson, S. I. Ou, P. Lito, K. P. Papadopoulos, P. A. Jänne, P. Olson, J. G. Christensen, The $KRAS^{G12C}$ inhibitor MRTX849 provides insight toward therapeutic susceptibility of KRAS-mutant cancers in mouse models and patients. *Cancer Discov.* **10**, 54–71 (2020). doi:10.1158/2159-8290.CD-19-1167 Medline

17. J. Y. Xue, Y. Zhao, J. Aronowitz, T. T. Mai, A. Vides, B. Qeriqi, D. Kim, C. Li, E. de Stanchina, L. Mazutis, D. Risso, P. Lito, Rapid non-uniform adaptation to conformation-specific KRAS(G12C) inhibition. *Nature* **577**, 421–425 (2020). doi:10.1038/s41586-019-1884-x Medline

18. D. S. Hong, M. G. Fakih, J. H. Strickler, J. Desai, G. A. Durm, G. I. Shapiro, G. S. Falchook, T. J. Price, A. Sacher, C. S. Denlinger, Y.-J. Bang, G. K. Dy, J. C. Krauss, Y. Kuboki, J. C. Kuo, A. L. Coveler, K. Park, T. W. Kim, F. Barlesi, P. N. Munster, S. S. Ramalingam, T. F. Burns, F. Meric-Bernstam, H. Henary, J. Ngang, G. Ngarmchamnanrith, J. Kim, B. E. Houk, J. Canon, J. R. Lipford, G. Friberg, P. Lito, R. Govindan, B. T. Li, $KRAS^{G12C}$ inhibition with sotorasib in advanced solid tumors. *N. Engl. J. Med.* **383**, 1207–1217 (2020). doi:10.1056/NEJMoa1917239 Medline

19. J. C. Hunter, A. Manandhar, M. A. Carrasco, D. Gurbani, S. Gondi, K. D. Westover, Biochemical and structural analysis of common cancer-associated KRAS mutations. *Mol. Cancer Res.* **13**, 1325–1335 (2015). doi:10.1158/1541-7786.MCR-15-0203 Medline

20. B. E. Hall, D. Bar-Sagi, N. Nassar, The structural basis for the transition from Ras-GTP to Ras-GDP. *Proc. Natl. Acad. Sci. U.S.A.* **99**, 12138–12142 (2002). doi:10.1073/pnas.192453199 Medline

21. N. Watson, M. E. Linder, K. M. Druey, J. H. Kehrl, K. J. Blumer, RGS family members: GTPase-activating proteins for heterotrimeric G-protein alpha-subunits. *Nature* **383**, 172–175 (1996). doi:10.1038/383172a0 Medline

22. E. M. Ross, T. M. Wilkie, GTPase-activating proteins for heterotrimeric G proteins: Regulators of G protein signaling (RGS) and RGS-like proteins. *Annu. Rev. Biochem.* **69**, 795–827 (2000). doi:10.1146/annurev.biochem.69.1.795 Medline

23. R. R. Neubig, D. P. Siderovski, Regulators of G-protein signalling as new central nervous system drug targets. *Nat. Rev. Drug Discov.* **1**, 187–197 (2002). doi:10.1038/nrd747 Medline

24. J. J. Tesmer, D. M. Berman, A. G. Gilman, S. R. Sprang, Structure of RGS4 bound to AlF4—activated G(i alpha1): Stabilization of the transition state for GTP hydrolysis. *Cell* **89**, 251–261 (1997). doi:10.1016/S0092-8674(00)80204-4 Medline

25. S. P. Srinivasa, N. Watson, M. C. Overton, K. J. Blumer, Mechanism of RGS4, a GTPase-activating protein for G protein alpha subunits. *J. Biol. Chem.* **273**, 1529–1533 (1998). doi:10.1074/jbc.273.3.1529 Medline

26. D. Rabara, T. H. Tran, S. Dharmaiah, R. M. Stephens, F. McCormick, D. K. Simanshu, M. Holderfield, KRAS G13D sensitivity to neurofibromin-mediated GTP hydrolysis. *Proc. Natl. Acad. Sci. U.S.A.* **116**, 22122–22131 (2019). doi:10.1073/pnas.1908353116 Medline

27. L. Rezabkova, E. Boura, P. Herman, J. Vecer, L. Bourova, M. Sulc, P. Svoboda, V. Obsilova, T. Obsil, 14-3-3 protein interacts with and affects the structure of RGS domain of regulator of G protein signaling 3 (RGS3). *J. Struct. Biol.* **170**, 451–461 (2010). doi:10.1016/j.jsb.2010.03.009 Medline

28. O. Daumke, M. Weyand, P. P. Chakrabarti, I. R. Vetter, A. Wittinghofer, The GTPase-activating protein Rap1GAP uses a catalytic asparagine. *Nature* **429**, 197–201 (2004). doi:10.1038/nature02505 Medline

29. Y. Li, K. Inoki, K. L. Guan, Biochemical and functional characterizations of small GTPase Rheb and TSC2 GAP activity. *Mol. Cell. Biol.* **24**, 7965–7975 (2004). doi:10.1128/MCB.24.18.7965-7975.2004 Medline

30. N. Sunaga, D. S. Shames, L. Girard, M. Peyton, J. E. Larsen, H. Imai, J. Soh, M. Sato, N. Yanagitani, K. Kaira, Y. Xie, A. F. Gazdar, M. Mori, J. D. Minna, Knockdown of oncogenic KRAS in non-small cell lung cancers suppresses tumor growth and sensitizes tumor cells to targeted therapy. *Mol. Cancer Ther.* **10**, 336–346 (2011). doi:10.1158/1535-7163.MCT-10-0750 Medline

31. J. B. Gibbs, M. D. Schaber, W. J. Allard, I. S. Sigal, E. M. Scolnick, Purification of ras GTPase activating protein from bovine brain. *Proc. Natl. Acad. Sci. U.S.A.* **85**, 5026–5030 (1988). doi:10.1073/pnas.85.14.5026 Medline

32. M. R. Webb, A continuous spectrophotometric assay for inorganic phosphate and for measuring phosphate release kinetics in biological systems. *Proc. Natl. Acad. Sci. U.S.A.* **89**, 4884–4887 (1992). doi:10.1073/pnas.89.11.4884 Medline

33. P. Lito, A. Saborowski, J. Yue, M. Solomon, E. Joseph, S. Gadal, M. Saborowski, E. Kastenhuber, C. Fellmann, K. Ohara, K. Morikami, T. Miura, C. Lukacs, N. Ishii, S. Lowe, N. Rosen, Disruption of CRAF-mediated MEK activation is required for effective MEK inhibition in KRAS mutant tumors. *Cancer Cell* **25**, 697–710 (2014). doi:10.1016/j.ccr.2014.03.011 Medline

34. A. M. Waters, I. Ozkan-Dagliyan, A. V. Vaseva, N. Fer, L. A. Strathern, G. A. Hobbs, B. Tessier-Cloutier, W. K. Gillette, R. Bagni, G. R. Whiteley, J. L. Hartley, F. McCormick, A. D. Cox, P. J. Houghton, D. G. Huntsman, M. R. Philips, C. J. Der, Evaluation of the

selectivity and sensitivity of isoform- and mutation-specific RAS antibodies. *Sci. Signal.* **10**, eaao3332 (2017). doi:10.1126/scisignal.aao3332 Medline

35. P. Bankhead, M. B. Loughrey, J. A. Fernández, Y. Dombrowski, D. G. McArt, P. D. Dunne, S. McQuaid, R. T. Gray, L. J. Murray, H. G. Coleman, J. A. James, M. Salto-Tellez, P. W. Hamilton, QuPath: Open source software for digital pathology image analysis. *Sci. Rep.* **7**, 16878 (2017). doi:10.1038/s41598-017-17204-5 Medline

36. Y. Xue, L. Martelotto, T. Baslan, A. Vides, M. Solomon, T. T. Mai, N. Chaudhary, G. J. Riely, B. T. Li, K. Scott, F. Cechhi, U. Stierner, K. Chadalavada, E. de Stanchina, S. Schwartz, T. Hembrough, G. Nanjangud, M. F. Berger, J. Nilsson, S. W. Lowe, J. S. Reis-Filho, N. Rosen, P. Lito, An approach to suppress the evolution of resistance in $BRAF^{V600E}$-mutant cancer. *Nat. Med.* **23**, 929–937 (2017). doi:10.1038/nm.4369 Medline

37. M. H. Hofmann, M. Gmachl, J. Ramharter, F. Savarese, D. Gerlach, J. R. Marszalek, M. P. Sanderson, D. Kessler, F. Trapani, H. Arnhof, K. Rumpel, D.-A. Botesteanu, P. Ettmayer, T. Gerstberger, C. Kofink, T. Wunberg, A. Zoephel, S.-C. Fu, J. L. Teh, J. Böttcher, N. Pototschnig, F. Schachinger, K. Schipany, S. Lieb, C. P. Vellano, J. C. O'Connell, R. L. Mendes, J. Moll, M. Petronczki, T. P. Heffernan, M. Pearson, D. B. McConnell, N. Kraut, BI-3406, a potent and selective SOS1-KRAS interaction inhibitor, is effective in KRAS-driven cancers through combined MEK inhibition. *Cancer Discov.* **11**, 142–157 (2021). doi:10.1158/2159-8290.CD-20-0142 Medline